



Supplement of

Variability of depolarization of aerosol particles in the megacity of Beijing: implications for the interaction between anthropogenic pollutants and mineral dust particles

Yu Tian et al.

Correspondence to: Xiaole Pan (panxiaole@mail.iap.ac.cn)

The copyright of individual parts of the supplement might differ from the CC BY 4.0 License.

Supplementary

Tables

Table S1: Wind degree and corresponding wind speed.

Wind degree	0	1	2	3	4	5	6	7	8	9	10	11	12
Wind speed (m/s)	0.0-0 .2	0.3-1 .5	1.6-3 .3	3.4-5 .4	5.5-7 .9	8.0-1 0.7	10.8- 13.8	13.9- 17.1	17.2- 20.7	20.8- 24.4	24.5- 28.4	28.5- 32.6	32.7- 36.9

Figures

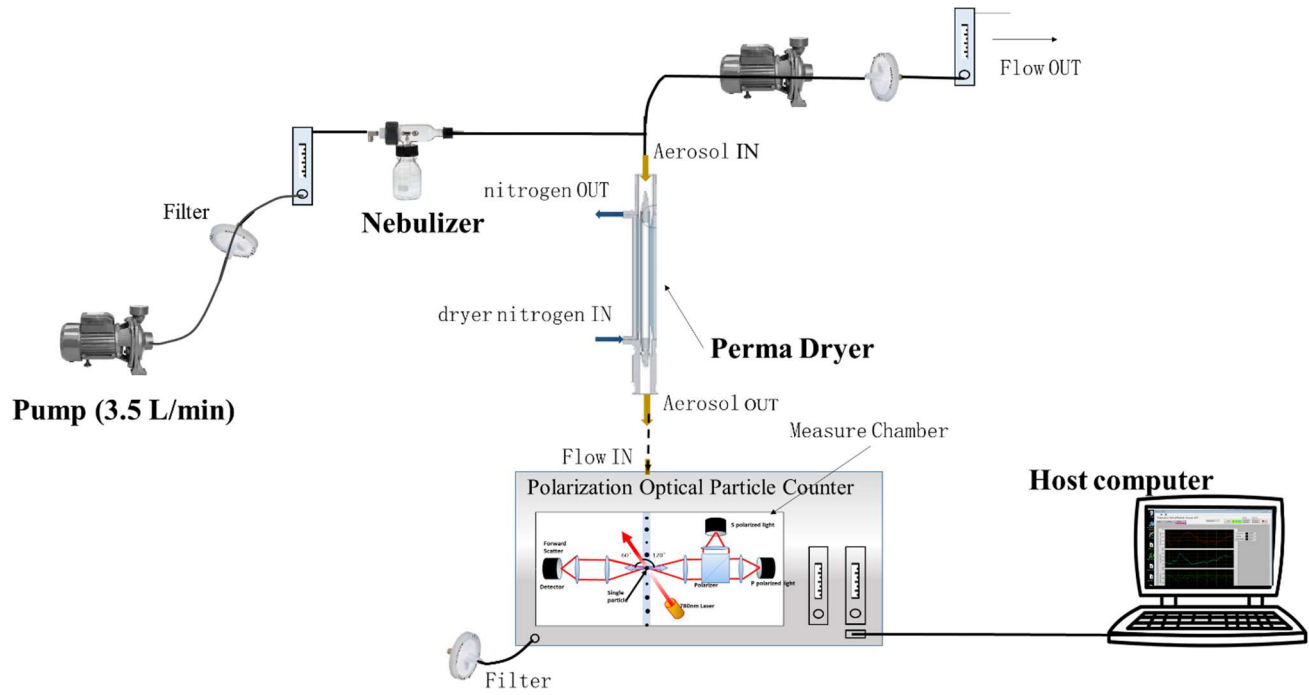


Figure S1. A schematic diagram of the laboratory calibration process.

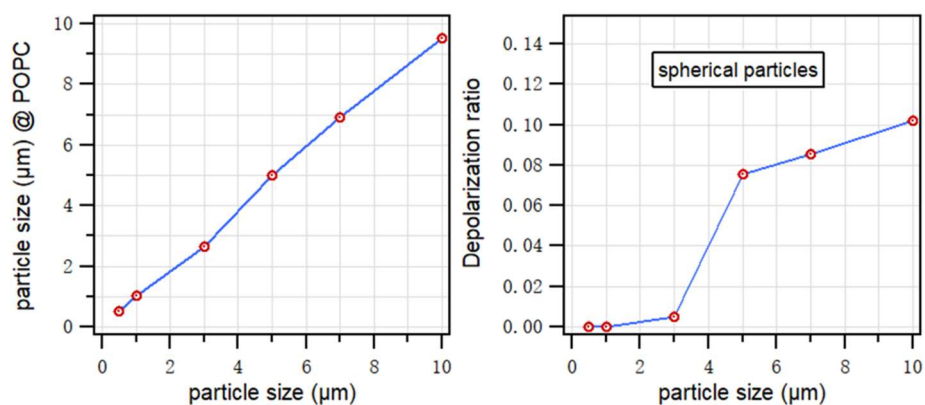


Figure S2. The calibration results of POPC using spherical polystyrene standard aerosols at $D_p = 0.048 \mu\text{m}$, $1.005 \mu\text{m}$, $3.210 \mu\text{m}$, $5.125 \mu\text{m}$, $7.008 \mu\text{m}$, $10.14 \mu\text{m}$. Optical size of the particle derived from a forward scattering signal at 60 degree (left); Depolarization ratio of the standard particles detected from a backward scattering signal at 120 degree (right).

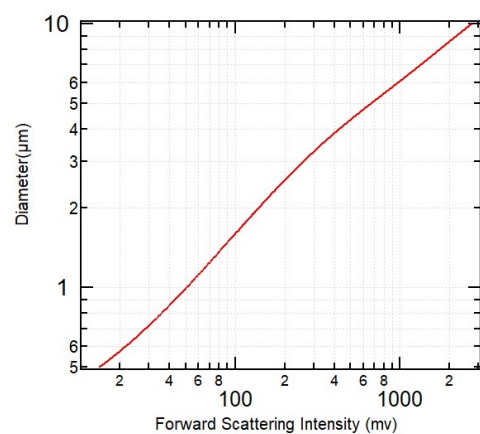


Figure S3. Calibration curve between forward scattering intensity and standard spherical particles' diameter.

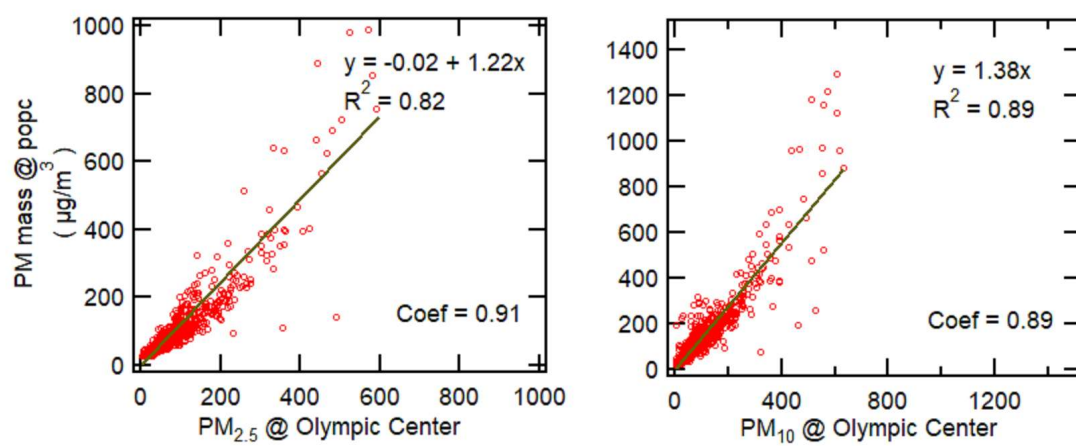


Figure S4: Comparison of the POPC derived particle concentration and observation data from Olympic Center state control site at the same time.

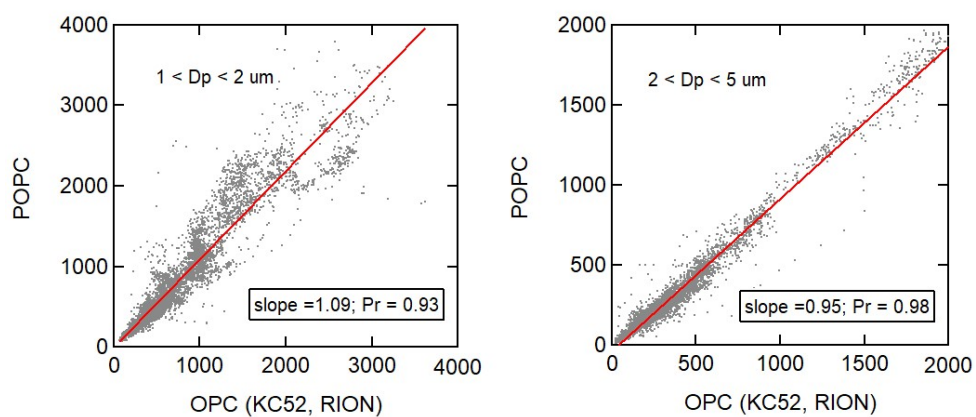


Figure S5. The comparison of number concentrations measured by POPC and OPC (KC52, RION).

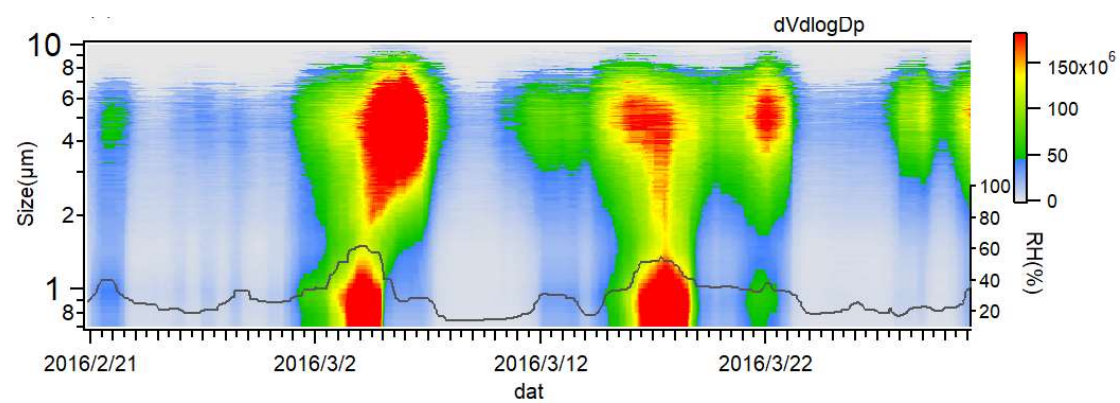


Figure S6. Volume size distribution of aerosols from February 21 to March 29, 2016.

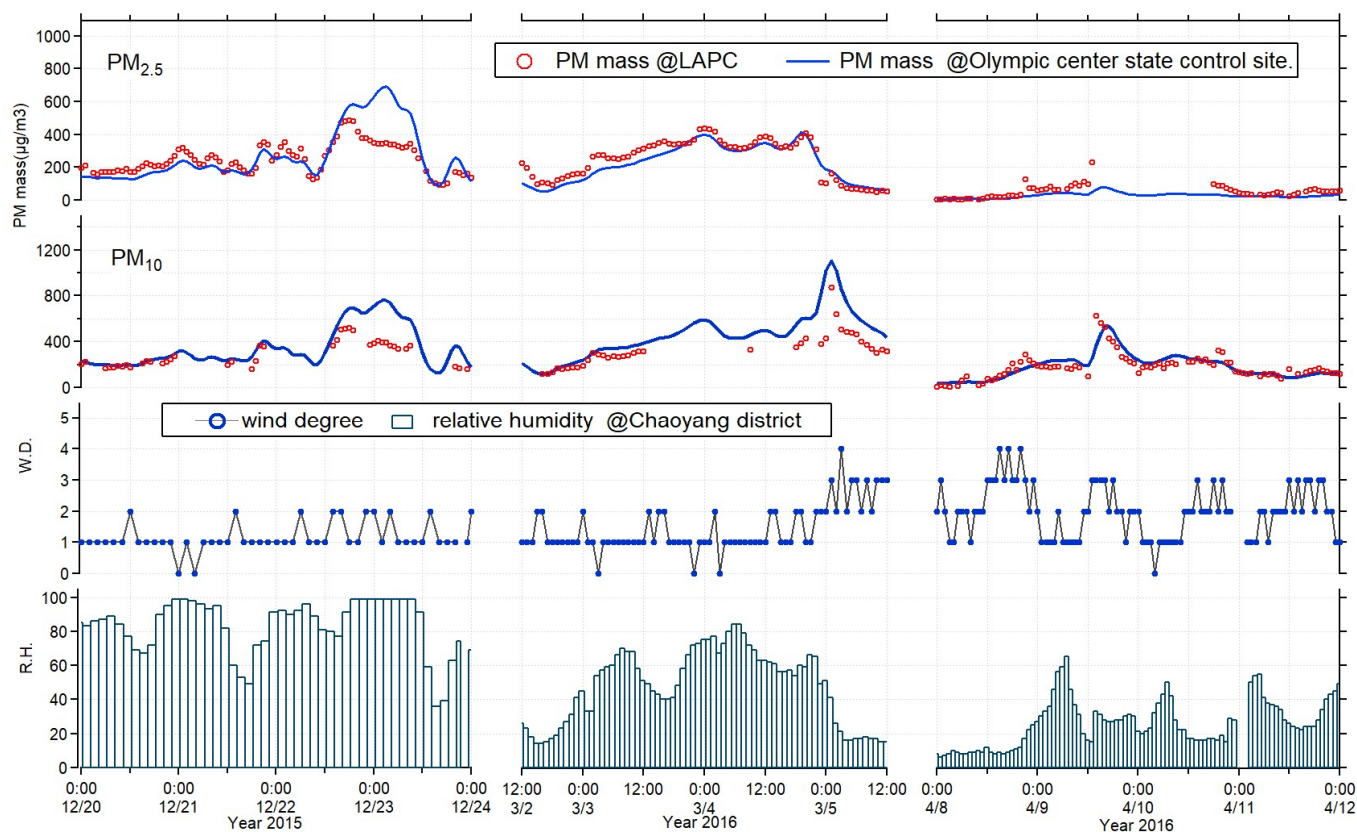


Figure S7: Key meteorological factors and the air quality index during the mixing pollution period: $\text{PM}_{2.5}$; PM_{10} ; W.D. represents the wind degree (corresponding table of specific wind degree and wind speed data is shown as Table S1); R.H. represents relative humidity (%).

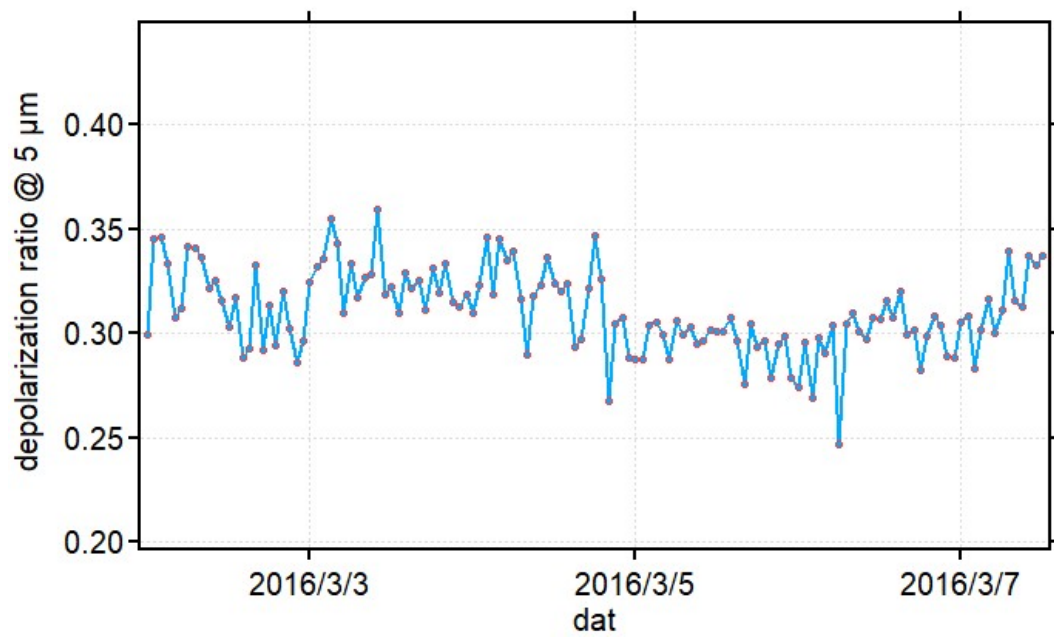


Figure S8. Depolarization ratio for 5 μm particles during case C.

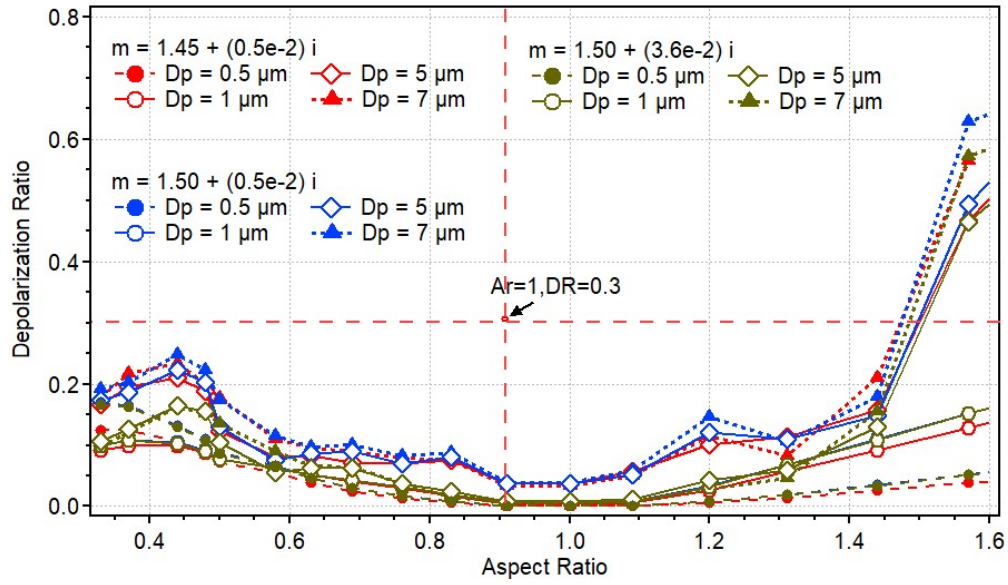


Figure S9. Teoretical simulation of the depolarization ratio of randomly oriented elongated ellipsoid particles as a function of the aspect ratio at fine mode: $D_p = 0.5 \mu\text{m}$, $D_p = 1 \mu\text{m}$, and $D_p = 5 \mu\text{m}$, $7 \mu\text{m}$ and on the basis of the T-matrix methodology.

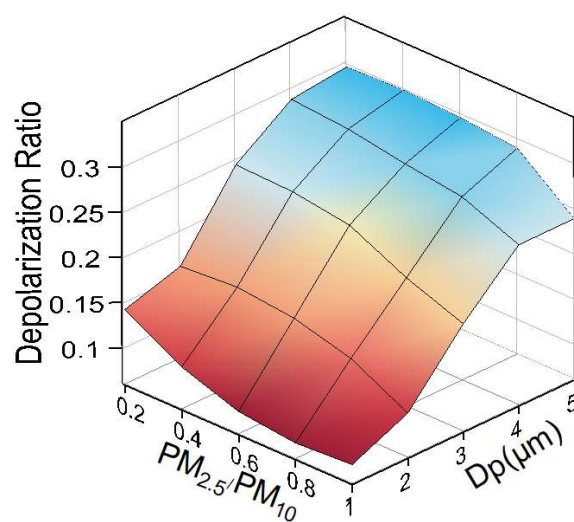


Figure S10. Surface plot of the depolarization ratio as a function of particle size (from 1 μm to 5 μm) and $PM_{2.5}/PM_{10}$ (from 0.2 to 1).

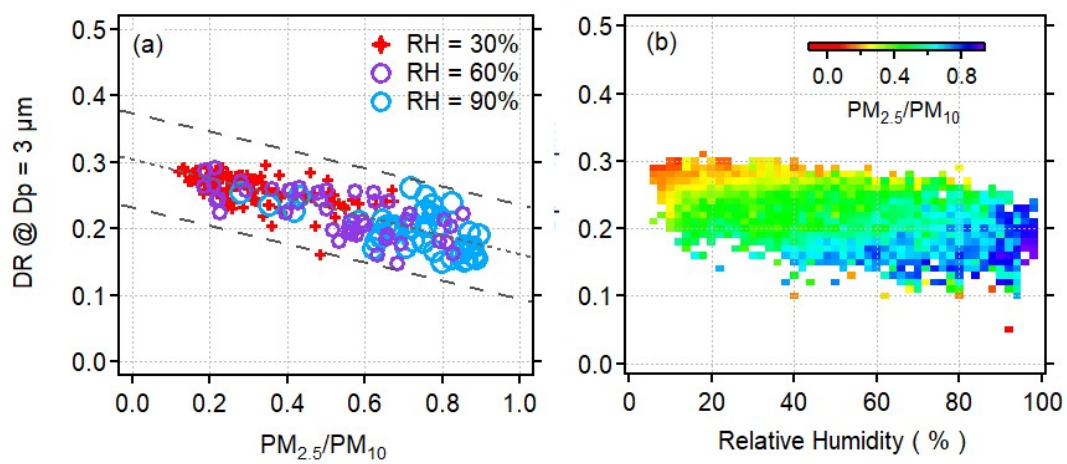


Figure S11. Scatter diagram of the relationship between the δ value of dust particles (at $D_p = 3 \mu\text{m}$), vapor content (RH) and $\text{PM}_{2.5}/\text{PM}_{10}$ in the air.

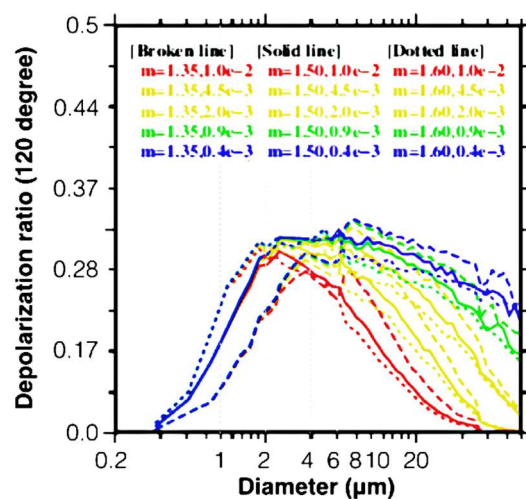


Figure S12. Theoretical calculation of depolarization ratio (at 120 backward direction) as a function of particle size for different refractive index.